J Mater Sci (2009) 44:6144–6148
DOI 10.1007/s10853-009-3849-1

Hydrothermal synthesis of amorphous spherical-shaped $YBO_3:Eu^{3+}$ and its photoluminescence property

Dalai Jin · Xiaojing Yu · Xiaoqin Xu · Lina Wang · Longcheng Wang · Naiyan Wang

Received: 17 April 2009 / Accepted: 25 August 2009 / Published online: 3 September 2009

Abstract Amorphous spherical Eu doped YBO_3 was synthesized by a mild one-step hydrothermal method. X-ray diffraction (XRD) and scanning electron microscope (SEM) were used to characterize the as-prepared products. It was demonstrated that the use of urea as alkali source plays the key function in the formation of amorphous spherical $YBO_3:Eu^{3+}$. The crystallinity and the morphologies of the $YBO_3:Eu^{3+}$ were sensitive to the urea content and the hydrothermal time. Room temperature photoluminescence (PL) spectra were detected. The sample in uniform diameter of 300–400 nm had the relative strong red emissions (*R*) and *R*/*O* ratio of 1.3.

Introduction

$YBO_3:Eu^{3+}$ has received much more attentions recently as candidate for plasma display panels (PDP) and a possible new material of Hg-free fluorescent lamps, due to its high vacuum ultraviolet (VUV) transparency and exceptional optical damage threshold [1–5]. The luminance property of PDP phosphor materials is strongly affected by the particle size and morphology [6]. Surface perfect and spherical-shaped phosphor always has high packing density, good slurry property, and smoother light intensity distribution. It can enhance the luminescent intensity and optimize the optical and geometrical structure of phosphor layers [7–9]. Moreover, the ultra-fine phosphor particles with very small size can potentially lead to higher screen resolution, lower screen loading, and a higher screen density.

The characteristic emission of $YBO_3:Eu^{3+}$ is composed of almost equal contributions of $^5D_0 \rightarrow {}^7F_1$ and $^5D_0 \rightarrow {}^7F_2$ transitions, which give rise to an orange–red emission instead of red and thus hampers its application. The latter transitions are hypersensitive to the symmetry of the local crystal fields surrounding the Eu^{3+} ions, and they are relatively strong when the symmetry of the crystal field is relatively low. It is of challenge in preparing spherical-shaped $YBO_3:Eu^{3+}$ with relative strong red emission.

Since the crystallization and structure of the material may have significant influence on its spectroscopic properties, various methods have been employed to synthesize the $YBO_3:Eu^{3+}$ with different crystallinity, morphology and size, such as co-precipitation method [10], solid-state reaction method [11], sol–gel method [12, 13], sol–gel pyrolysis process [14, 15], etc., obtaining single crystal or powder materials with micron or nanometer size. But the amorphous material was seldom researched on its morphology and spectroscopic property. Hydrothermal synthesis method here is advanced to be a simple, practical, and cost-effective route which is reported before to be used to obtain, $(Y,Gd)BO_3:Eu^{3+}$ [16, 17], $YBO_3:Tb^{3+}$ [18] and so on. It is of the advantage in preparing ultra-fine particles with uniform morphology and narrow size distribution.

Here in our paper, a mild hydrothermal method was applied to synthesize $YBO_3:Eu^{3+}$ composites with various morphologies. It proved that amorphous spherical-shaped

D. Jin (✉) · X. Yu · X. Xu · L. Wang · N. Wang
Center of Materials Engineering, Zhejiang Sci-Tech University, Xiasha University Town, 310018 Hangzhou, People's Republic of China
e-mail: jdl_zist@126.com

L. Wang
Key Laboratory of Advanced Textile Materials and Manufacturing Technology, Ministry of Education, Zhejiang Sci-Tech University, 310018 Hangzhou, People's Republic of China

YBO_3:Eu^{3+} with relative strong red emission was obtained by using urea as alkali source. The selected alkali source and the reaction parameters played important roles in crystallization and structure determination of the material.

Experiment

All the reagents were of analytical grade and used without any further purification. Boric acid was first dissolved in the distilled water to form 3 mmol/L solution. Then certain amount of the mixture of $Y(NO_3)_3$ and $Eu(NO_3)_3$ was co-added into above solution under magnetic stirring condition. The molar ratio of B/(Y + Eu) was 1:1. Then, certain amount of urea was introduced to the above solution under stirring. The initial pH value was around four when urea was introduced and no precipitate was formed. The resulting solution was poured into a 100 mL capacity teflon-lined stainless steel autoclave and sealed. The autoclave was heated to the desired temperature for certain time, and then cooled down naturally to room temperature. The pH value of the solution before and after the hydrothermal reaction was detected as listed in Table 1. The product was then collected by centrifugation, washed with deoinized water for several times, and air-dried at 60 °C for 24 h for characterization. NH_4OH and NaOH were chosen as the alkali sources, respectively, for comparison research, and white precipitate appeared immediately at the stage of the adding of NH_4OH or NaOH.

The phase structure and phase purity of the as-synthesized products were examined by a high-resolution Thermo ARL X'TRA X-ray diffractometer at the step size of 0.02° and scanning speed of 1° min^{-1} using Cu Kα radiation ($\lambda = 0.15418$ nm). The morphologies and the sizes of the products were observed by a Hitachi S-4700 field-emission scanning electron microscope. The photoluminescence (PL) spectra were measured at room temperature on a Hitachi F-4600 fluorescence-spectrophotometer equipped with a 150 W xenon lamp as the excitation source. The work voltage was 400 V.

Results and discussion

The XRD patterns of the constituent products using different alkali sources are shown in Fig. 1. Only the amorphous phase is accessible with the urea addition as shown in Fig. 1a. With increasing the urea up to 1.2 g, and with the prolonging of the hydrothermal time up to 10 h, some degree of crystallinity takes place as shown in Fig. 1b, c. It is found that the samples are well-crystallized by using NH_4OH or NaOH. The inset of Fig. 1 shows that the constituent products are phase-pure vaterite-type YBO_3 (JCPDS no. 16-0277, hexagonal phase, space group $P6_3c$). The relative intensity of the peaks in these two patterns varies with each other obviously. The broad peaks as labeled by asterisks according to the XRD patterns suggest the nano-size of the samples. Compared with the standard diffraction pattern of YBO_3, there are small shifts to the lower 2-theta side. It can be attributed to the embedded Eu^{3+} ions into the host crystal lattice, which have greater ionic radius than that of Y^{3+} ions.

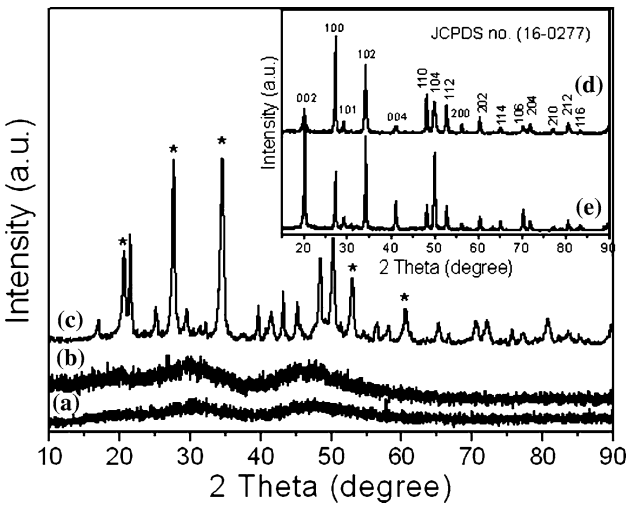

Fig. 1 XRD patterns of YBO_3:Eu^{3+} samples. The reaction parameters are (*a*) 0.6 g urea, 10 h; (*b*) 1.2 g urea, 8 h; (*c*) 1.2 g urea, 10 h. The inset on the *top right* is the XRD patterns of comparison YBO_3:Eu^{3+} samples using (*d*) NaOH and (*e*) NH_4OH, 1 h

Table 1 The pH value of the solution before and after the hydrothermal reaction

Alkali source	Alkali quantity (g)	pH value		Morphology
		Before hydrothermal reaction	After hydrothermal reaction	
Urea	0.6	4.34	8.66	Sphere
Urea	1.2	4.35	8.81	Sphere, flake
$NH_3 \cdot H_2O$	–	9.30	8.61	Flake
NaOH	–	9.00	4.66	Big sphere
NaOH	–	9.30	6.14	Sheet

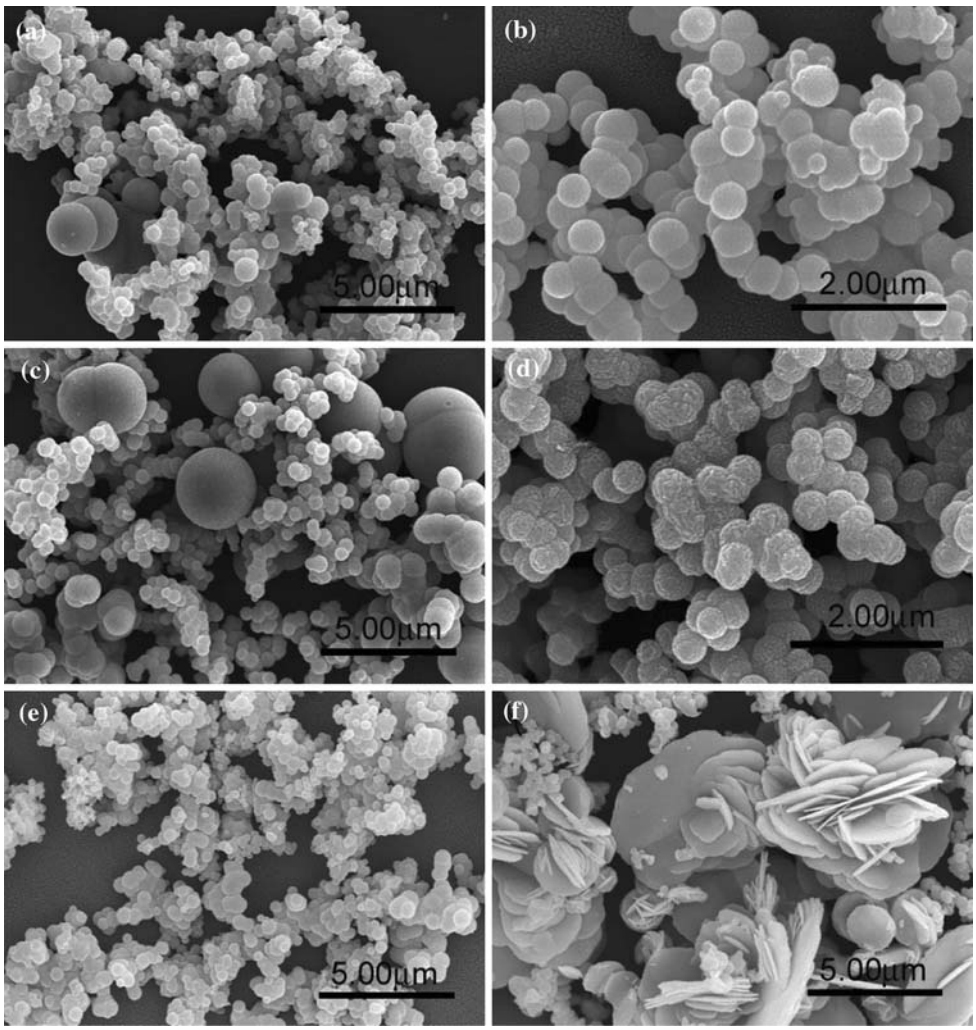

Fig. 2 SEM images of $YBO_3:Eu^{3+}$ samples. The reaction parameters are **a** 0.6 g urea, 1 h; **b** 1.2 g urea, 1 h; **c** 0.6 g urea, 8 h; **d** 1.2 g urea, 8 h; **e** 0.6 g urea, 10 h; **f** 1.2 g urea, 10 h

Figure 2 shows the general morphologies of the $YBO_3:Eu^{3+}$ samples using various urea contents. Spherical-shaped sample with broad grain size-distribution is obtained as the content was 0.6 g at the hydrothermal time of 1 h. With the increase of the content and/or with the prolonging of the hydrothermal reaction time, the sizes of the balls turn to be homogeneous with narrower distribution. Well shaped sphericity in homogeneous size of 300–400 nm is obtained as the content was 1.2 g at the hydrothermal time of 8 h as shown in Fig. 2d. Once the phase of the sample is crystallized as proved by XRD, flake-formed crystals appear as shown in Fig. 2f.

Morphologies of the comparison samples are also observed by SEM as shown in Fig. 3 The samples obtained by using NH_4OH and NaOH have much larger size compared with that in Fig. 2. Sheet-like crystals are obtained when controlling the initial pH value of 9.30. The sheets are in better dispersivity as NaOH is used, which are about 20 μm in diameter and several tens nanometer in thickness. Interestingly, big spherical crystals are synthesized when the initial pH is controlled at 9.0 using NaOH. The spheres are about some tens micron in diameter and the sub-crystalline is fringy like.

The room temperature PL spectra are measured as shown in Fig. 4. Strong emissions from the $^5D_0 \rightarrow {}^7F_J$ (J = 0–2) transition of Eu^{3+} activators are identified in all samples. The red emissions (*R*) ($^5D_0 \rightarrow {}^7F_2$) range from 610 to 630 nm, and the orange emissions (*O*) ($^5D_0 \rightarrow {}^7F_1$) are centered at about 598 nm. The amorphous spherical $YBO_3:Eu^{3+}$ samples have dominative red emission (*R*) which is advantage for its application as three basic colors phosphor (TBCP). The intensity ratio of the *R*/*O* reaches to 1.3 after 8 h of hydrothermal reaction. With the recombination of the atoms from disorder to regularity as detected by XRD, the red emission (*R*) decreases instead with the crystallized sample as shown in Fig. 4a. As it has been reported mostly that large crystals with well crystallinity have stronger luminescence behavior, so this is a challenge for nano-sized phosphors. Here in this paper, the amorphous spherical $YBO_3:Eu^{3+}$ samples have relative strong

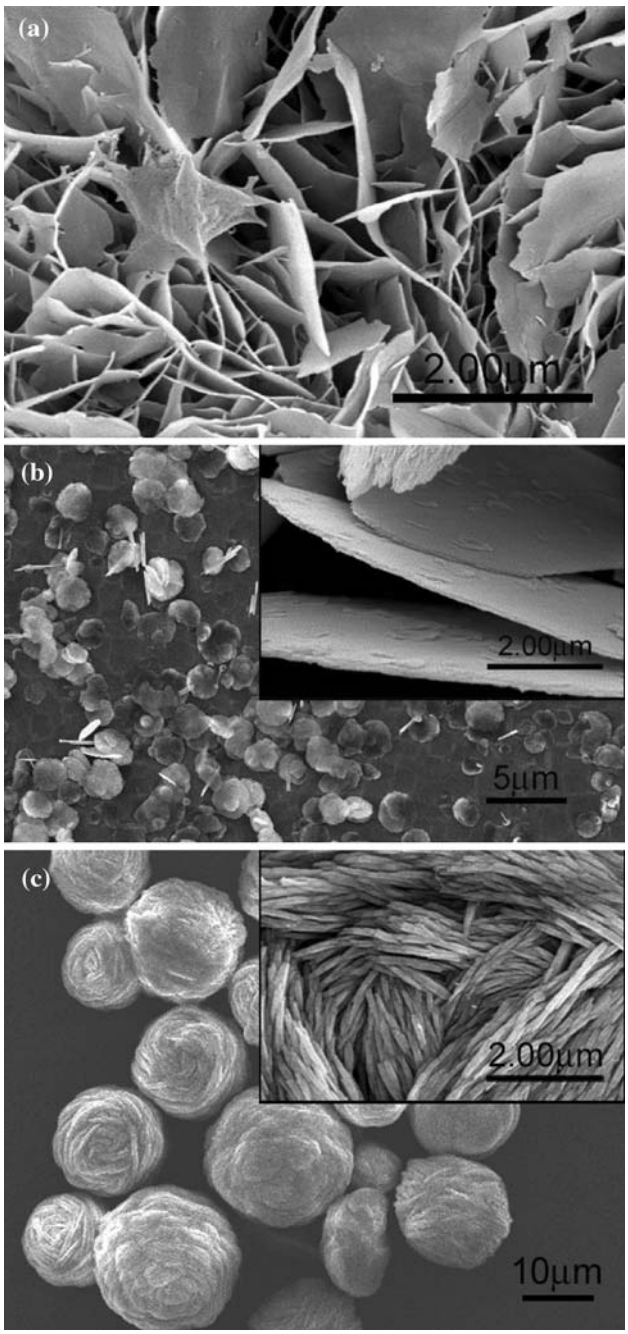

Fig. 3 SEM images of comparison $YBO_3:Eu^{3+}$ samples under the reaction parameters of **a** NH_4OH, initial pH = 9.30; **b** NaOH, initial pH = 9.30; **c** NaOH, initial pH = 9.0. Inset shows the high-magnification SEM image of the sample

red emission (*R*), which is quite similar with that for the comparison samples. Although the larger samples obtained using NH_4OH and NaOH have relative strong PL intensity, it is accompanied with unexpected high *O*/*R* ratio. Similar phenomenon was also reported by Zhang et al. [19] that the effect of crystal disorder increased the *R*/*O*.

It is confirmed by our experiments that the alkali source is absolutely necessary for the formation of the borate salt. As for the roles of the alkali in the reaction, it is suggested as follows.

During the hydrothermal synthesis process, the raw material boric acid is first dissolved in the water to perform a Lewis acid by combining with the H_2O molecule. It is considered that the borate radical should be released after some neutralization reactions. The OH^- concentration is then important to determine the rate of the hydrothermal reaction. In our experiments, different alkalis are selected. NaOH is a strong base, ionizes completely. While NH_4OH is a weak alkali and will only ionize partially depending on the ionization equilibrium. Urea releases OH^- only after heating where the decomposition equilibrium is temperature dependent. Thus, the OH^- feeding rate during the hydrothermal process is conferred to be $V_{NaOH} > V_{NH_4OH} > V_{urea}$. The slowest reaction rate using urea causes the uniform spherical shape of the product in nano-size and its uncompleted crystallization in amorphous state. As a result, the red emission from electric dipole $^5D_0 \rightarrow {}^7F_2$ transition is relatively strong, which is allowed in the inner electronic configuration and is hardly influenced by the environment of the Eu^{3+} activators [20, 21]. Once the sample crystallized under the certain condition, such as more addition of urea or prolonging the hydrothermal time, the orange emission from magnetic dipole $^5D_0 \rightarrow {}^7F_1$ increases. It proves by most of the literatures that the transition probabilities of $^5D_0 \rightarrow {}^7F_1$ magnetic dipole increase when the Eu^{3+} located at an inversion symmetry center of S_6 symmetry [1, 3], which is the site of the Y^{3+} in YBO_3 crystal.

Conclusion

$YBO_3:Eu^{3+}$ with various morphologies and crystallinity was synthesized by a mild hydrothermal method. It proved by XRD and SEM measurements that the structure of the samples was hypersensitive with the used alkali sources. Amorphous $YBO_3:Eu^{3+}$ with spherical shape in uniform size of 300–400 nm was obtained by using urea. Flake-shaped particle was formed when the particle got crystallization. Much larger crystals were obtained by using NaOH and NH_4OH. It was considered that the OH^- feeding rate during the hydrothermal process influenced the crystallization process and resulted in the final morphologies. Room temperature PL spectra showed that the amorphous spherical-shaped $YBO_3:Eu^{3+}$ sample had strong emission intensity with the intensity ratio of *R*/*O* reached to 1.3. It is an ideal candidate for phosphor application.

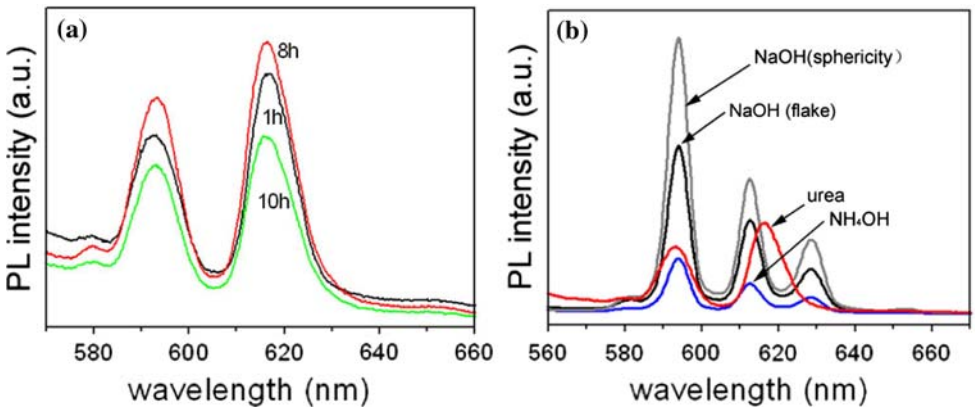

Fig. 4 Photoluminescence spectra of $YBO_3:Eu^{3+}$ samples prepared by **a** using 0.6 g urea under different hydrothermal time; **b** using different alkali sources

Acknowledgement This work is supported by Science Foundation of Zhejiang Sci-Tech University (ZSTU) under Grant No.111383A4Y 06054.

References

1. Joffin N, Caillier B, Garcia A, Guillot P, Galy J, Fernandes A, Mauricot R, Dexpert-Ghys J (2006) Opt Mater 28(6–7):597
2. Wei ZG, Sun LD, Liao CS, Yin JL, Jiang XC, Yan CH (2002) J Phys Chem B 106(43):11085
3. Wei ZG, Sun LD, Liao CS, Jiang XC, Yan CH, Tao Y, Hou XY, Ju X (2003) J Appl Phys 93(12):9783
4. Lin JH, Sheptyakov D, Wang Y, Allenspach P (2004) Chem Mater 16:2418
5. Wang Y, Wang L (2006) Mater Lett 60(21–22):2645
6. Kang YC, Lenggoro IW, Okuyama K, Park SB (1999) J Electrochem Soc 146(3):1227
7. Sievers RE, Milewski PD, Xu CY, Watkins BA (1997) In: Proceedings of the 3rd international conference on the science and technology of display phosphors, p 303
8. Okazaki C, Shiiki M, Suzuki T, Suzuki K (2000) J Lumin 87–89:1280
9. Tanaka S, Ozaki I, Kunimoto T, Ohmi K, Kobayashi H (2000) J Lumin 87–89:1250
10. Yadav RS, Dutta RK, Kumar M, Pandey AC (2009) J Lumin 129(9):1078
11. Lemanceau S, Bertrand-Chadeyron G, Mahiou R, El-Ghozzi M, Cousseins JC, Conflant P, Vannier RN (1999) J Solid State Chem 148:229
12. Jiang XC, Sun LD, Feng W, Yan CH (2004) Cryst Growth Des 4(3):517
13. Boyer D, Bertrand G, Mahiou R (2003) J Lumin 104:229
14. Wei ZG, Sun LD, Liao CS, Yin JL, Jiang XC, Yan CH, Lu SZ (2002) J Phys Chem B 106:10610
15. Wei ZG, Sun LD, Liao CS, Jiang XC, Yan CH (2002) J Mater Chem 12(12):3665
16. Guo X, Wang Y, Zhang J (2009) J Cryst Growth 311(8):2409
17. Wang YH, Endo T, He L, Wu CF (2004) J Cryst Growth 268 (3–4):568
18. Zhang JC, Wang YH, Guo X (2007) J Lumin 122–123:980
19. Zhang J, Lin J (2004) J Cryst Growth 271:207
20. Wei ZG, Sun LD, Liao CS, Yan CH (2002) Appl Phys Lett 80:1447
21. Judd BR (1962) Phys Rev 127:750